Supporting Information for

Microstructural origin of resistance-strain hysteresis in carbon nanotube thin film conductors

Lihua Jin[a,b], Alex Chortos[c], Feifei Lian[d], Eric Pop[d], Christian Linder[a],

Zhenan Bao[c], Wei Cai[e]

[a]Department of Civil and Environmental Engineering, Stanford University, Stanford, CA 94305, USA
[b]Department of Mechanical and Aerospace Engineering, University of California, Los Angeles, CA 90095, USA
[c]Department of Chemical Engineering, Stanford University, Stanford, CA 94305, USA
[d]Department of Electrical Engineering, Stanford University, Stanford, CA 94305, USA
[e]Department of Mechanical Engineering, Stanford University, Stanford, CA 94305, USA

S1. Pair potential for CGMS simulation

To understand the resistance-strain hysteresis of carbon nanotubes (CNTs) conductors, we use coarse-grained molecular statics (CGMS) method to simulate the morphological change of CNT networks under loading cycles. We model a thin sheet of CNTs composed of a collection of N_{CNT} nanotubes, with each one discretized by a set of (on the order of 100) N_{node} nodes. We use the following pair potential for different nodes (1, 2):

$$V(\{r_i, r_j\}) = \sum_i \frac{1}{2} k_s (|r_{i+1} - r_i| - l_0)^2 + \sum_i \frac{1}{2} k_B \left(\frac{(r_{i-1} - r_i) \cdot (r_{i+1} - r_i)}{|r_{i-1} - r_i| \cdot |r_{i+1} - r_i|} + 1 \right) + \sum_{i,j} \left(\frac{C_{12}}{(r_i - r_j)^{12}} - \frac{C_6}{(r_i - r_j)^6} \right). \quad \text{(S1)}$$

The first two terms are the stretching and bending energies between neighboring nodes in one CNT. The interaction parameters are chosen to reproduce the bending and stretching response of an elastic tube with Young's modulus $E_{CNT} = 5TPa$, inner diameter $d_{in} = d_{CNT} - h_{CNT}$, and outer diameter $d_{out} = d_{CNT} + h_{CNT}$, where d_{CNT} is the diameter of the CNTs, and we adopt the CNT wall thickness $h_{CNT} = 0.07$ nm (3). The parameters r_i in Eq. S1 is the position of a node, $l_0 = l_{CNT}/N_{node}$ is the stress-free length between two neighboring nodes, with l_{CNT} the length of CNTs. The stretching stiffness is $k_s = E_{CNT} A_{CNT}/l_0$ with the cross-section area $A_{CNT} = \pi\left(r_{out}^2 - r_{in}^2\right)/2$, and the bending stiffness is $k_s = E_{CNT} I_{CNT}/l_0$ with the moment of inertia $I_{CNT} = \pi\left(d_{out}^4 - d_{in}^4\right)/64$. The last term of Eq. S1 is the Lennard-Jones potential for non-neighboring nodes. The

parameters $C_{12} = N_c c_{12}$ and $C_6 = N_c c_6$, where N_c is the number of carbon atoms represented by each node (4), $c_{12} = 2516582.4\ \text{kcal}\cdot\text{mol}^{-1}\text{Å}^{12}$, and $c_6 = 1228.8\ \text{kcal}\cdot\text{mol}^{-1}\text{Å}^6$ (5). For single-wall CNTs, we estimate $N_c = \pi d_{CNT} l_0 / A_C$, where $A_C = 2.6194\ \text{Å}^2$ is the average area covered by each carbon atom. An additional potential is applied to each node to model the adhesion and repulsion of the substrate

$$U = \begin{cases} \frac{1}{2} k_1 (y - y_0)^2 & y \le y_0, \\ k_2 \left(1 - e^{-\frac{1}{2}(y-y_0)^2} \right) & y > y_0, \end{cases} \qquad \text{(S2)}$$

where y is the thickness direction of the CNT network, and y_0 is the position of the substrate. Here we set $k_1 = k_2 = k_s$. The initial simulation cell has the size of H_x, H_y = 100 nm and H_z in the x, y and z direction. Periodic boundary conditions are applied in the x and z directions, i.e. within the plane of the CNT film.

S2. Calculating the resistance of CNT networks

S2.1. Zero net current condition

According to Ohm's law, the electrical current I is proportional to the voltage difference across a conductor ΔV

$$I = G\Delta V, \qquad \text{(S3)}$$

where G is the conductance. Fig. Sec S1 sketches the electrical current through one CNT, which is discretized with multiple nodes. A voltage drop is applied at the two ends of the simulation cell. When the steady state is reached, net current going in and out each node is zero. Take node 3 as an example, and this condition can be expressed as

$$G_{32}(V_3 - V_2) + G_{34}(V_3 - V_4) = 0. \qquad \text{(S4)}$$

This can be reorganized as

$$(G_{32} + G_{34})V_3 - G_{32}V_2 - G_{34}V_4 = 0. \qquad \text{(S5)}$$

The general condition of zero net current for node i is

$$\sum_j G_{ij} V_i - \sum_j G_{ij} V_j = 0, \qquad \text{(S6)}$$

where nodes j are the ones connecting node i.

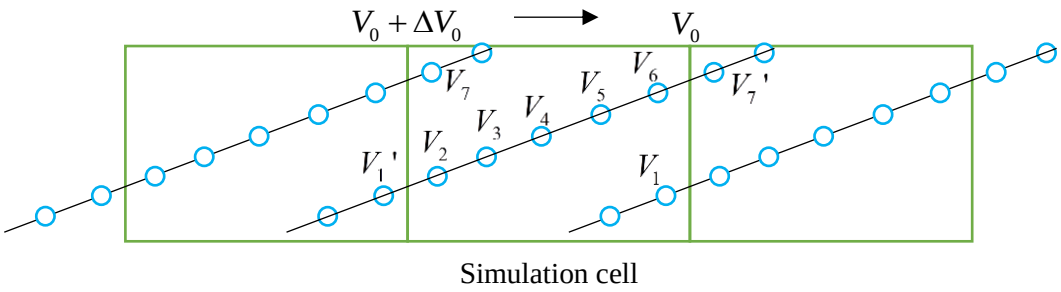

Fig. Sec S1. Schematics of the current through the nodes of a CNT in the simulation cell and the two neighboring unit cells under the periodic boundary condition.

S2.2. Periodic boundary condition

Since the period boundary condition is applied to the simulation cell and a voltage difference ΔV_0 is applied at the two ends of the simulation cell, the voltage of node 1 in the simulation cell and node 1' which physically connected to node 2 (Fig. Sec S1) satisfies the relation

$$V_1' = V_1 + \Delta V_0 \ . \qquad \text{(S7)}$$

The zero net current condition for node 2 is

$$G_{21}(V_2 - V_1') + G_{23}(V_2 - V_3) = 0 \ , \qquad \text{(S8)}$$

which can be rewritten as the same form of Eq. S6, but with a source term $G_{21}\Delta V_0$

$$G_{21}(V_2 - V_1) + G_{23}(V_2 - V_3) = G_{21}\Delta V_0 \ . \qquad \text{(S9)}$$

Similarly, the zero net current condition for node 6 can be written as the general form with a source term $-G_{67}\Delta V_0$

$$G_{65}(V_6 - V_5) + G_{67}(V_6 - V_7) = -G_{67}\Delta V_0 \ . \qquad \text{(S10)}$$

Thus, the zero net flux conditions for the node i connecting their neighbors on the left boundary of the simulation cell introduce a source term $\sum_j G_{ij}\Delta V_0$, while the zero net flux conditions for the node connecting their neighbors on the right boundary introduce a source term $-\sum_j G_{ij}\Delta V_0$.

S2.3. Contact resistance

So far, we have only considered resistance to current of bonded nodes inside one CNT. When two CNTs contact, a larger contact resistance needs to be considered. If nodes i and k form a contact, the zero net current condition of node i should be modified as

$$\sum_j G_{ij}V_i - \sum_j G_{ij}V_j + \sum_k \tilde{G}_{ik}V_i - \sum_k \tilde{G}_{ik}V_k = 0 \ , \quad \text{(S11)}$$

where $\tilde{G}_{ik}$ is the contact conductance, which is usually much smaller than G_{ij}, the conductance between bonded nodes. Similarly, for the contacts formed on the boundary of the simulation cell, source terms need to be added as shown in Eqs. S9 and S10.

S2.4. Governing equation set

Considering the zero net current condition for all the nodes ($i = 1$ to n), we obtain a governing equation set

$$\mathbf{GV} = \mathbf{S} , \quad \text{(S12)}$$

with voltage $\mathbf{V} = (V_i)_{n\times 1} = \left(V_1, V_2, \ldots V_n\right)^T$, source term $\mathbf{S} = (S_i)_{n\times 1} = \left(S_1, S_2, \ldots S_n\right)^T$ and the conductance matrix $\mathbf{G} = (G_{ij})_{n\times n}$. S_i becomes nonzero if node i connects their neighbors or forms contacts on the left or right boundaries of the simulation cell. G_{ij} becomes nonzero if nodes i and j form a bond or contact. Under the given voltage drop on the boundary of the simulation cell ΔV_0, the conductance between bonded or contacting nodes G_{ij} and $\tilde{G}_{ij}$, and the known structure of the CNT network, we can solve Eq. S12 and obtain the distribution of the voltage in the simulation cell.

Next, in order to calculate the effective conductance of the CNT network, we need to calculate the total current going through the simulation cell. To do so, we can choose an arbitrary cross-section, and the total current across it should be independent of the choice. Here we just take the left boundary of the simulation cell as an example. For a node i connecting its neighboring node j across the left boundary, the current across the boundary can be calculated as

$$I_{ij} = G_{ij}(V_j + \Delta V_0 - V_i) \ . \quad \text{(S13)}$$

The total flux can then be obtained as the sum of all flux through bonded CNTs I_{ij} and contacts $\tilde{I}_{ik}$, $I = \sum_{i,j,k} I_{ij} + \tilde{I}_{ik}$. The effective conductance of the matrix can be calculated as $G = I / \Delta V_0$, and the effective resistance as $R = 1/G$. The electric conductance through

bonded CNTs G_{ij} are related to the CNT resistance as $G_{ij} = 1/R_{node}$, and the electric conductance through contacts $\tilde{G}_{ij}$ are related to the contact resistance as $\tilde{G}_{ij} = 1/R_{contact}$.

S3. Analytical model of resistance evolution under loading cycles

Here we establish an analytical model to relate the resistances in the stretching and transverse directions, R_x and R_z respectively, with the loading history in the limit of very long CNTs, which easily buckles under compression. In this model, we first obtain an expression for the dependence of the mean relative projected length ξ on the strain history, and then establish the relation between ξ and the electrical resistance R.

Before stretching, the CNTs are assumed to be straight, with a random distribution of orientation. Therefore, the mean relative projected length $\xi_x = \langle l_x \rangle / h_x$ and $\xi_z = \langle l_z \rangle / h_z$ before stretching are

$$\frac{\xi_{x0} H_x}{l_{CNT}} = \frac{\xi_{z0} H_z}{l_{CNT}} = \frac{2}{\pi} \int_0^{\pi/2} \cos\Theta d\Theta = 0.637 , \qquad \text{(S14)}$$

where H_x and H_z are the sizes of the simulation cell in *x* and *z* directions before the stretching, l_{CNT} is the length of CNTs, and Θ is the angle between the CNT and the *x* axis.

After stretching, the CNTs may be curved, and we consider the vector connecting the two end points of every CNT, the end-to-end vector. If the end-to-end vector deforms affinely with the applied strain, it experiences a stretch of $\lambda = 1 + \varepsilon$ in the *x* direction, and a stretch of $1/\sqrt{\lambda}$ in the *z* direction. Then the vector of a CNT with the initial orientation Θ deforms to length l_{aff}, and rotates to orientation θ

$$l_{aff} = l_{CNT} \sqrt{\lambda^2 \cos^2\Theta + \sin^2\Theta / \lambda} , \ \theta = \arctan\left(\tan(\Theta)\lambda^{-3/2}\right). \qquad \text{(S15)}$$

By setting $l_{aff} = l_{CNT}$, we can obtain a critical angle $\Theta_c = \arccos\left(1/\left(\lambda^2 + \lambda + 1\right)\right)$. For all CNTs with the initial orientation angle $\Theta > \Theta_c$, the length of the end-to-end vector becomes shorter under the affine deformation $l_{aff} < l_{CNT}$, and therefore we assume that all these CNTs buckle so that the end-to-end vectors will deform affinely with the applied strain. On the other hand, the end-to-end vector will not be able to follow the affine

deformation for all CNTs with the initial orientation angle $\Theta < \Theta_c$, since doing so would require the vector to become longer than the contour length of the CNT. For simplicity, we assume that the end-to-end vector for these CNTs will only rotate to the new orientation specified by the affine deformation, but its length will remain at the contour length of the CNT. Given these assumptions, during loading the mean relative projected length ξ_x and ξ_z can be expressed as

$$\xi_x = \frac{2}{\pi h_x}\left(l_{CNT}\int_0^{\Theta_c}\cos\theta d\Theta + l_{aff}\int_{\Theta_c}^{\pi/2}\cos\theta d\Theta\right), \qquad \text{(S16)}$$

$$\xi_z = \frac{2}{\pi h_z}\left(l_{CNT}\int_0^{\Theta_c}\sin\theta d\Theta + l_{aff}\int_{\Theta_c}^{\pi/2}\sin\theta d\Theta\right), \qquad \text{(S17)}$$

where the current simulation cell sizes relate the one before stretching by $h_x = \lambda H_x$ and $h_z = H_z / \sqrt{\lambda}$.

During unloading, after reaching the maximal stretch λ_{m}, the CNTs with $\Theta > \Theta_c$ reversibly recover from the buckling, and therefore the two ends of the CNTs always deform affinely with the substrate. It can also be proved that CNTs with initial orientation $\Theta < \Theta_c$ buckle during unloading, so the two ends of the CNTs follow the affine deformation of the substrate with the configuration under the maximal stretch λ_{m} as the reference state. During unloading, the mean relative projected length ξ_x and ξ_z can be calculated as

$$\xi_x = \frac{2}{\pi h_x}\left(l_{CNT}\int_0^{\Theta_c}\cos\theta_{\mathrm{m}}\frac{\lambda}{\lambda_{\mathrm{m}}}d\Theta + l_{aff}\int_{\Theta_c}^{\pi/2}\cos\theta d\Theta\right), \qquad \text{(S18)}$$

$$\xi_z = \frac{2}{\pi h_z}\left(l_{CNT}\int_0^{\Theta_c}\sin\theta_{\mathrm{m}}\sqrt{\frac{\lambda_{\mathrm{m}}}{\lambda}}d\Theta + l_{aff}\int_{\Theta_c}^{\pi/2}\sin\theta d\Theta\right), \qquad \text{(S19)}$$

where $\theta_{\mathrm{m}} = \arctan\left(\tan(\Theta)\lambda_{\mathrm{m}}^{-3/2}\right)$. Combining Eqs. S16-S19, we obtain Eq. 1 and 2 in the main text.

During the subsequent loading, the CNTs with $\Theta > \Theta_c$ will buckle again, while the CNTs with $\Theta < \Theta_c$ reversibly recover from the buckling until λ_{m}, after which Eqs. S16

and S17 are applicable again. Therefore, the subsequent reloading curve of $\xi - \varepsilon$ overlaps the unloading one until the previous maximal strain is reached.

After obtaining the evolution of ξ_x and ξ_z, we further relate them to R_x and R_z. The inverse of the mean relative projected length $\eta_x = h_x / \langle l_x \rangle$ represents the least contacts needed for electrons to conduct through the simulation cell in the *x* direction. Then N_{CNT} number of CNTs can form N_{CNT} / η_x parallel paths of conduction, so the resistance R_x should be proportional to η_x^2 / N_{CNT}. When the contact resistance $R_{contact}$ is much higher than the resistance of the CNTs, the resistance in the stretching direction can be estimated as

$$R_x = \alpha R_{contact} \eta_x^2 / N_{CNT}, \qquad \text{(S20)}$$

where α is a constant on the order of 1 related to the morphology of the CNT network. Similarly, the resistance in the z direction can be calculated as

$$R_z = \alpha R_{contact} \eta_z^2 / N_{CNT}. \qquad \text{(S21)}$$

Combining Eqs. S16-S21, we can analytically calculate the evolution of the resistance R_x and R_z with respect to an arbitrary loading history.

4. Supplementary figures

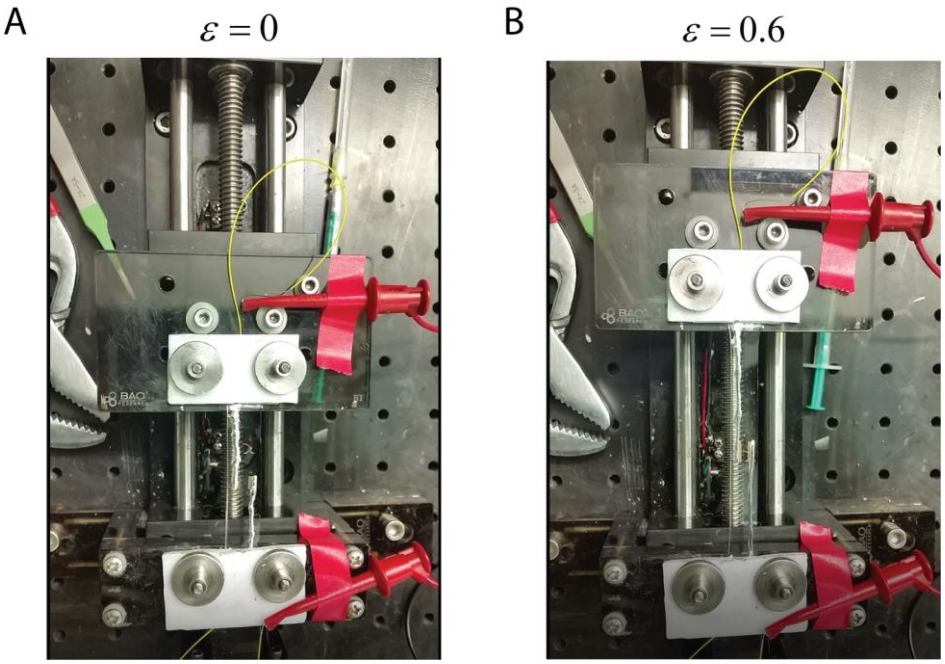

Fig. S1. Experimental setup for the *in situ* measurement of the resistance of the CNT thin film under a cyclic loading. (A) Images with no strain applied ($\varepsilon = 0$), and (B) with $\varepsilon = 0.6$. Analysis of the images (A) and (B) shows that the width and length changes of the PDMS substrate follow the one of an incompressible material under uniaxial deformation, and that the deformation of the CNT film is the same as the PDMS substrate.

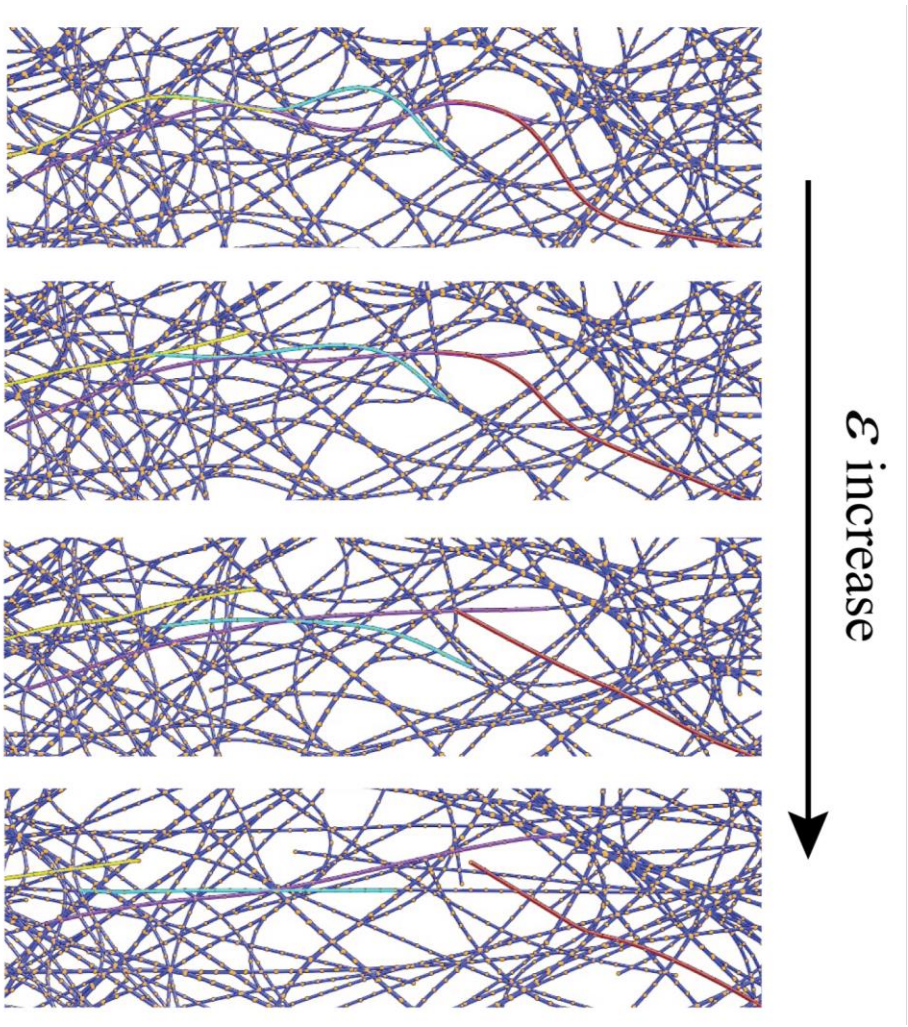

Fig. S2. Example of CNTs sliding in the same bundles as strain increases.

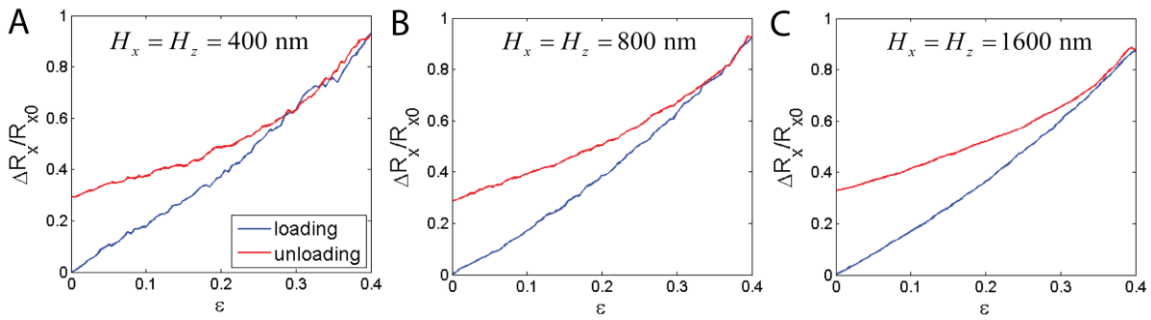

Fig. S3. Effect of the simulation cell size on the convergence of the simulation. The resistance of the CNT network increases and then decreases during a loading and unloading cycle of maximal strain 0.4, forming a hysteresis. Each CNT has length $l_{CNT} = 800$ nm and diameter $d_{CNT} = 1$ nm, and is discretized by $N_{node} = 40$ nodes. The simulation cell has size H_x and H_z in the x (loading) and z (transverse) directions, and 100 nm in the y direction. The cell size is varied from (A) $H_x = H_z = 400$ nm, (B) $H_x = H_z = 800$ nm, to (C) $H_x = H_z = 1600$ nm. The density of the CNTs is fixed, and the number of CNTs is (A) $N_{CNT} = 30$, (B) $N_{CNT} = 120$ and (C) $N_{CNT} = 480$ respectively. All the results shown here are the average of around 10 simulations. As we can see, even when the cell size is as small as half of the CNT length, the cell size almost does not affect the calculated resistance change.

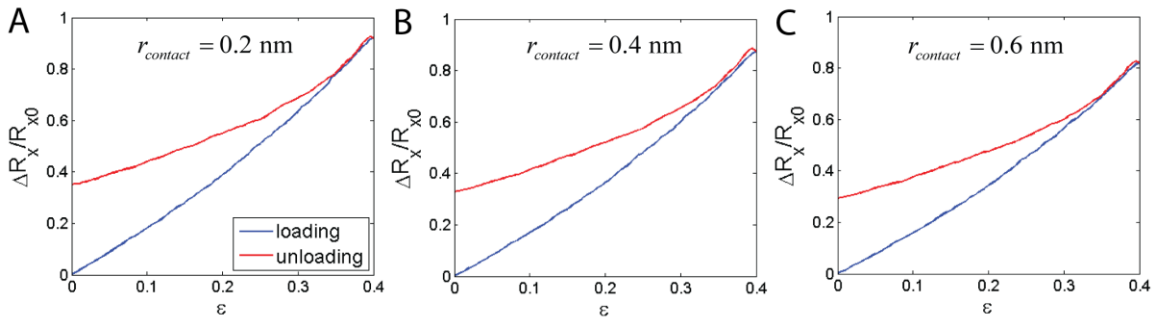

Fig. S4. Effect of the contact radius $r_{contact}$ on the convergence of the simulation, (A) $r_{contact} = 0.2$ nm, (B) $r_{contact} = 0.4$ nm, (C) $r_{contact} = 0.6$ nm. The CNT network is composed of $N_{CNT} = 480$ CNTs, each with length $l_{CNT} = 800$ nm, diameter $d_{CNT} = 1$ nm, and discretized by $N_{node} = 40$ nodes. As we can see, the resistance change is not sensitive to $r_{contact}$. In the following simulations, we always use $r_{contact} = 0.4$ nm.

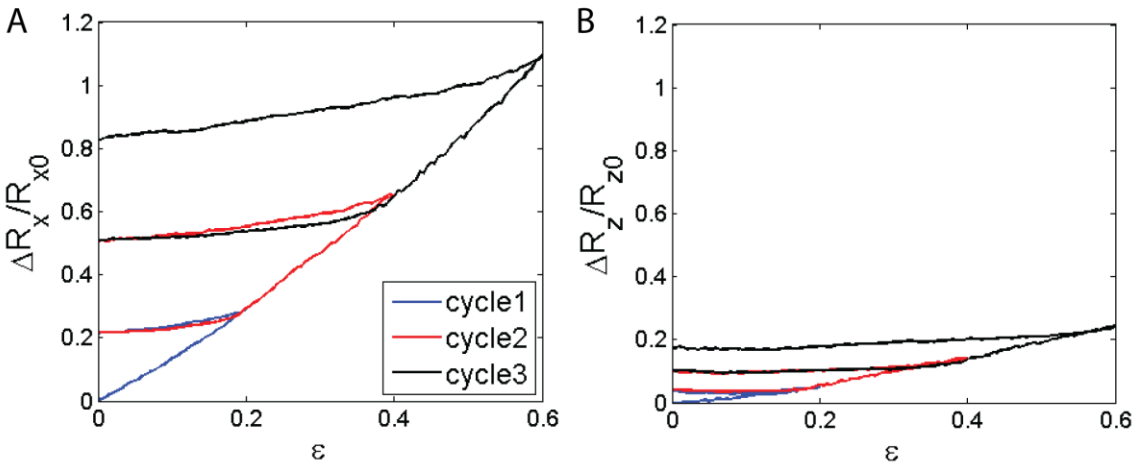

Fig. S5. A typical simulation result of the relative resistance change in the (A) *x* (loading) and (B) *z* (transverse) directions under three sequentially increasing strain cycles of 20%, 40% and 60% without averaging, for $N_{CNT}=135$ CNTs with length $l_{CNT}=2400$ nm, diameter $d_{CNT}=1$ nm, each discretized by $N_{node}=120$ nodes, in a simulation cell with $H_x=H_z=1200$ nm. The contact resistance is set as $R_{contact}=200$ kΩ, and the resistance of a single CNT is $R_{CNT}=17.3$ kΩ.

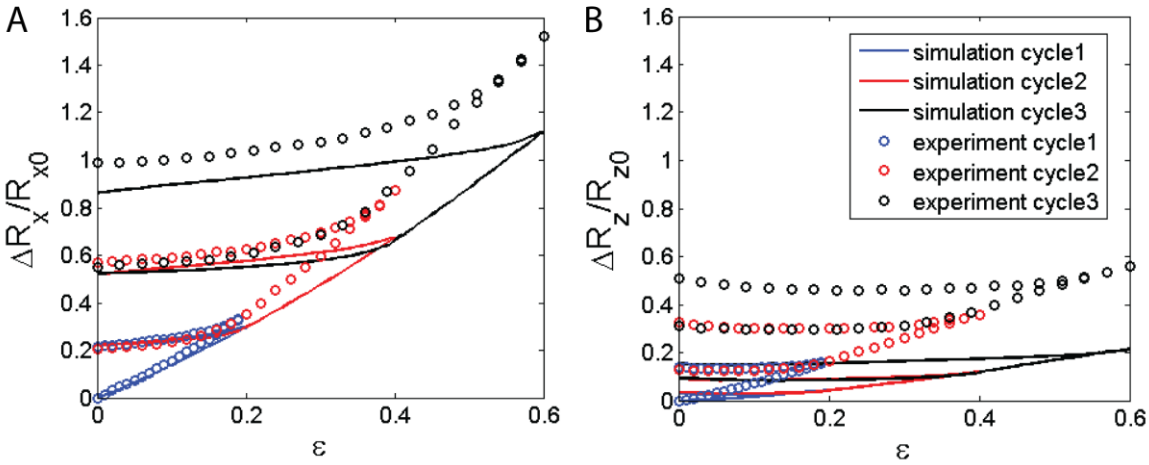

Fig. S6. Direct comparison between the CGMS simulation and the experimental results of the relative resistance change in the (A) *x* (loading) and (B) *z* (transverse) directions under three sequentially increasing strain cycles of 20%, 40% and 60%. The experimental and CGMS simulation results are shown in Fig. 2A, B and Fig. 2C, D respectively.

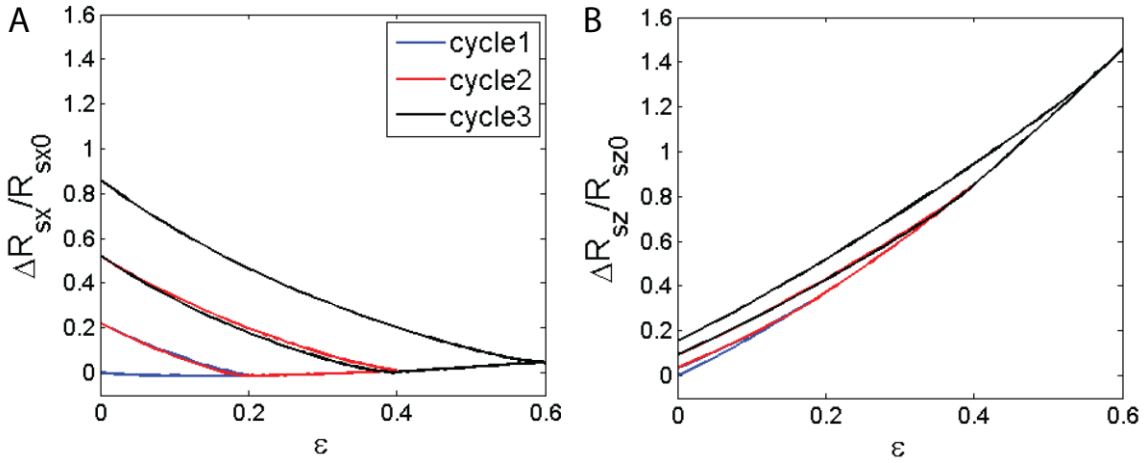

Fig. S7. The relative sheet resistance change in the (A) *x* and (B) *z* directions under three sequentially increasing strain cycles of 20%, 40% and 60%, for $N_{CNT}=135$ CNTs with length $l_{CNT}=2400$ nm, diameter $d_{CNT}=1$ nm, each discretized by $N_{node}=120$ nodes, in a simulation cell with $H_x=H_z=1200$ nm. Sheet resistance is defined as $R_{sx}=R_x h_z/h_x$ and $R_{sz}=R_z h_x/h_z$. The contact resistance is set as $R_{contact}=200$ kΩ, and the resistance of a single CNT is $R_{CNT}=17.3$ kΩ.

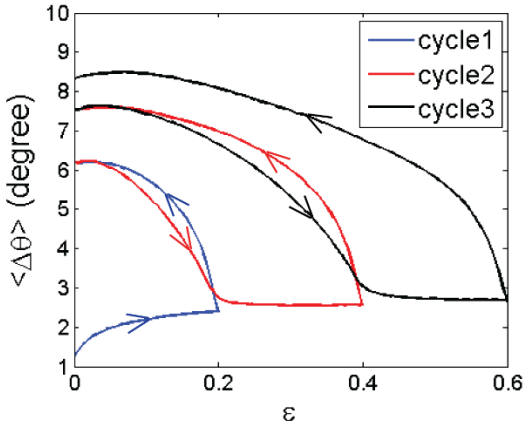

Fig. S8. Evolution of the mean angle difference between neighboring CNT segments $\langle \Delta\theta_{node} \rangle$ under three sequentially increasing strain cycles of 20%, 40% and 60%.

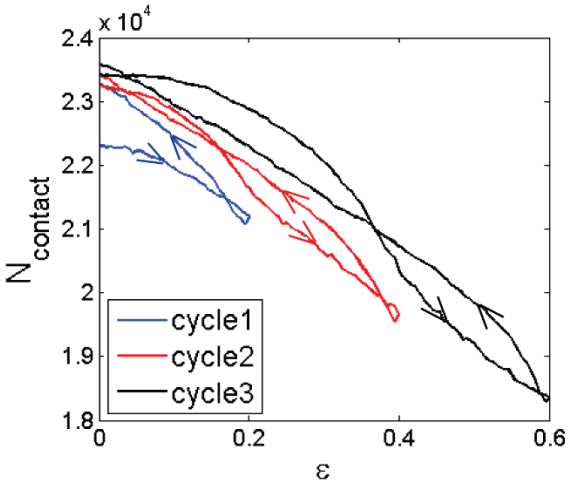

Fig. S9. Evolution of the number of total contacts $N_{contact}$ between CNTs under three sequentially increasing strain cycles of 20%, 40% and 60%.

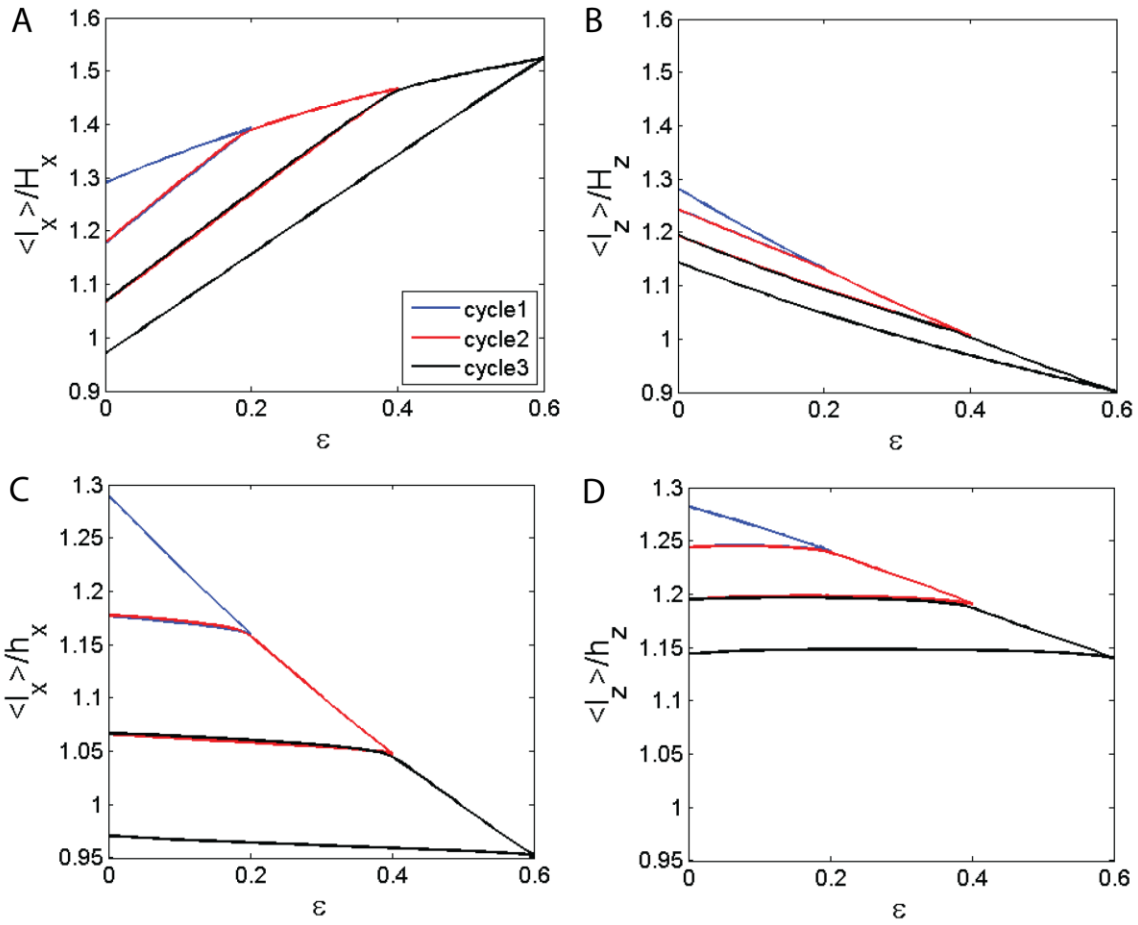

Fig. S10. The mean projected lengths of the end-to-end vectors of CNTs in the *x* and *z* directions normalized by the original simulation cell size (A, B) and the current cell size (C, D).

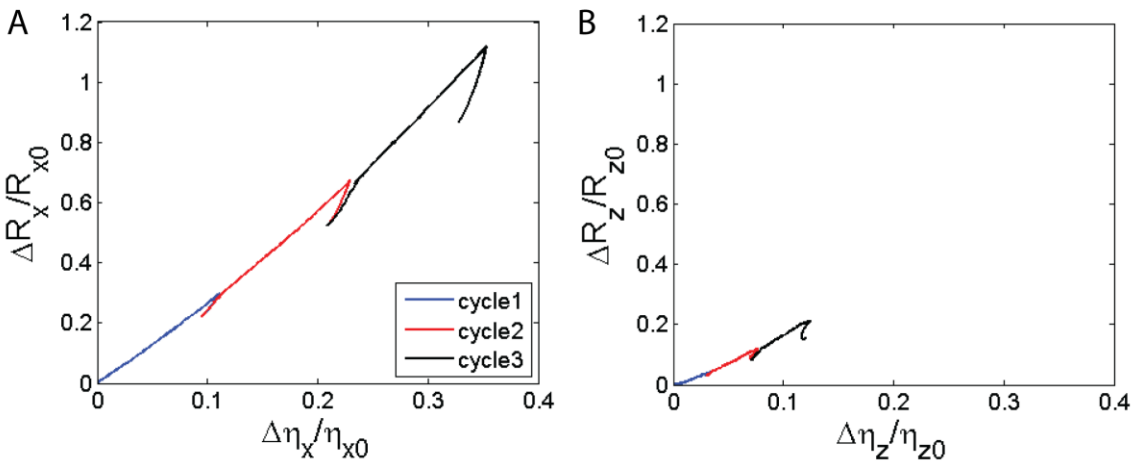

Fig. S11. The correlation of the relative resistance changes in the *x* direction $\Delta R_x / R_{x0}$ (A) and *z* direction $\Delta R_z / R_{z0}$ (B) with the relative changes of the inverse mean projected lengths in the *x* and *z* directions $\Delta \eta_x / \eta_{x0}$ and $\Delta \eta_z / \eta_{z0}$ respectively.

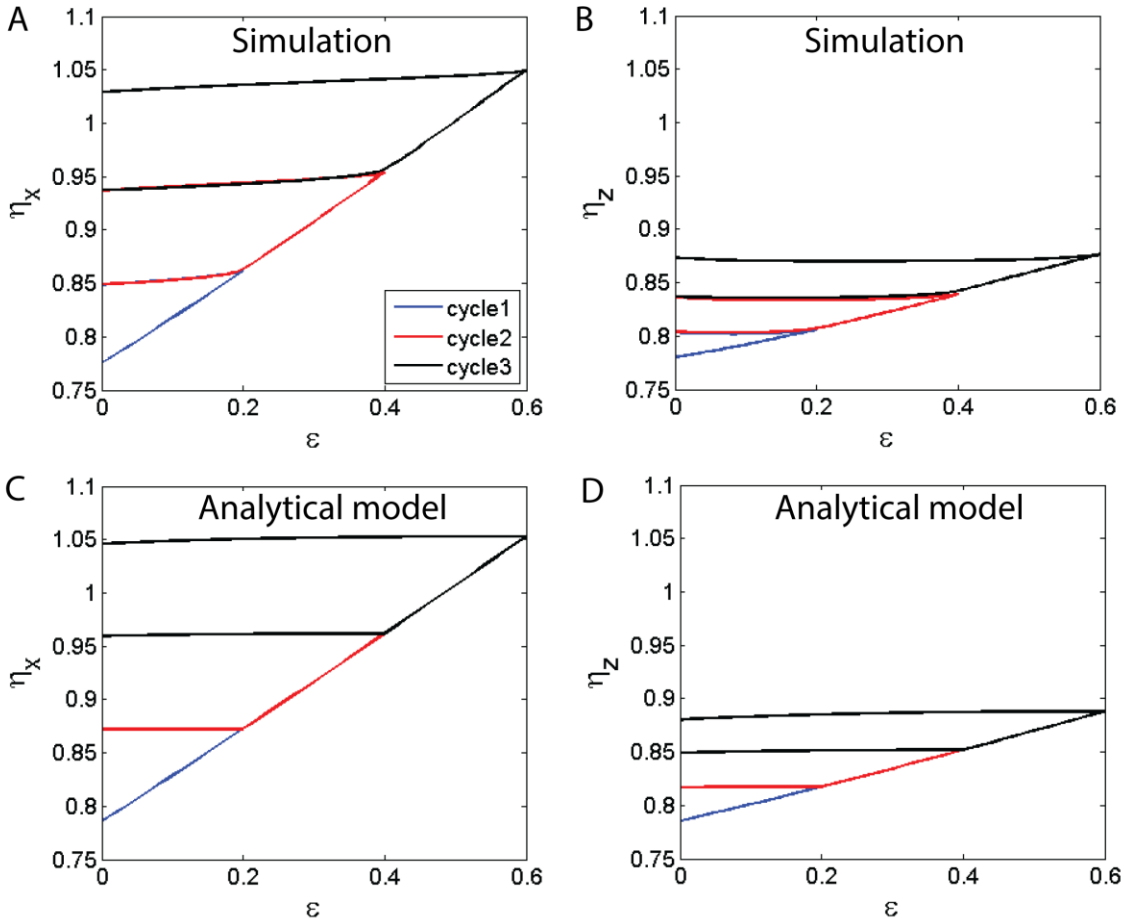

Fig. S12. The evolution of the inverse mean relative projected lengths in the x and z directions η_x (A, C) and η_z (B, D) by CGMS simulation (A, B) and analytical modeling (C, D). The simulation and analytical results show very good agreement.

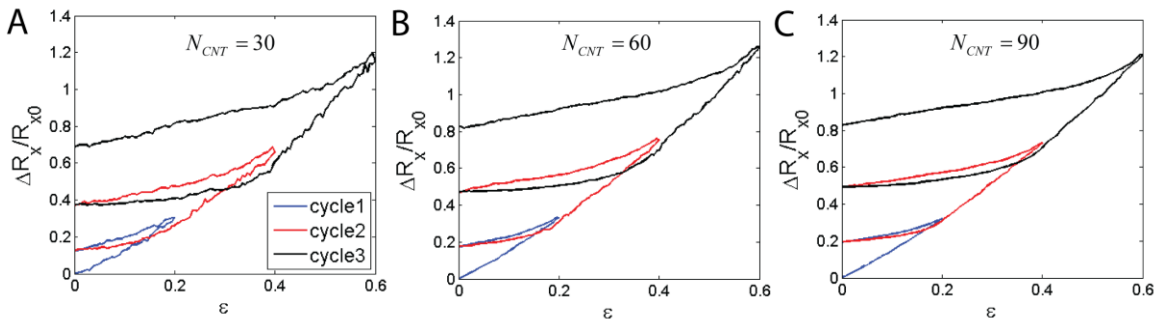

Fig. S13. Effect of CNT density on the evolution of the resistance change, (A) $N_{CNT}=30$ nanotubes, (B) $N_{CNT}=60$, (C) $N_{CNT}=90$. For all cases, the CNTs have length $l_{CNT}=1600$ nm, diameter $d_{CNT}=1$ nm, each discretized by $N_{node}=80$ nodes, in a simulation cell with $H_x=H_z=800$ nm.

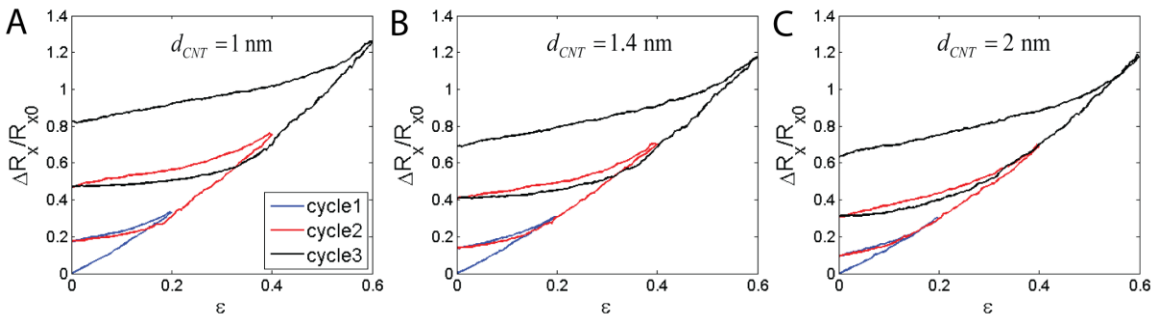

Fig. S14. Effect of the CNT diameter on the resistance change. (A) $d_{CNT} = 1$ nm, (B) $d_{CNT} = 1.4$ nm and (C) $d_{CNT} = 2$ nm. For all cases, the CNT network is composed of $N_{CNT} = 60$ CNTs, each with length $l_{CNT} = 1600$ nm, discretized by $N_{node} = 80$ nodes.

Movie S1. The evolution of the morphology of a CNT network under three sequentially increasing strain cycles of 20%, 40% and 60%. The CNT network is composed of $N_{CNT} = 135$ CNTs with length $l_{CNT} = 2400$ nm, diameter $d_{CNT} = 1$ nm, each discretized by $N_{node} = 120$ nodes, in a simulation cell with $H_x = H_z = 1200$ nm.

References

1. Buehler MJ (2006) Mesoscale modeling of mechanics of carbon nanotubes: self-assembly, self-folding, and fracture. *J Mater Res* 21(11):2855-2869.
2. Won Y, *et al.* (2013) Zipping, entanglement, and the elastic modulus of aligned single-walled carbon nanotube films. *P Natl Acad Sci USA* 110(51):20426-20430.
3. Yakobson BI, Brabec C, & Bernholc J (1996) Nanomechanics of carbon tubes: instabilities beyond linear response. *Phys Rev Lett* 76(14):2511.
4. Harik V (2002) Mechanics of carbon nanotubes: applicability of the continuum-beam models. *Comp Mater Sci* 24(3):328-342.
5. Jones J (1924) On the determination of molecular fields. III. From crystal measurements and kinetic theory data. *P Roy Soc Lond A Mat* 106(740):709-718.